Submitted to Acta Materialia

Interpretation of hydrogen-assisted fatigue crack propagation in BCC iron based on dislocation structure evolution around the crack wake

Domas Birenis[a], Yuhei Ogawa[b,c], Hisao Matsunaga[d,e,f], Osamu Takakuwa[e]

Junichiro Yamabe[e,f,g], Øystein Prytz[a], Annett Thøgersen[h]

[a] *Department of Physics, Centre for Materials Science and Nanotechnology, University of Oslo, PO Box 1048 - Blindern, NO-0316 Oslo, Norway*

[b] *Graduate School of Engineering, Kyushu University, 744 Motooka, Nishi-ku, Fukuoka 819-0395, Japan*

[c] *Research Fellow of the Japan Society for the Promotion of Science, 744 Motooka, Nishi-ku, Fukuoka 819-0395, Japan*

[d] *Department of Mechanical Engineering, Kyushu University, 744 Motooka, Nishi-ku, Fukuoka 819-0395, Japan*

[e] *Research Center for Hydrogen Industrial Use and Storage (HYDROGENIUS), Kyushu University, 744 Motooka, Nishi-ku, Fukuoka 819-0395, Japan*

[f] *International Institute for Carbon-Neutral Energy Research (I2CNER), Kyushu University, 744 Motooka, Nishi-ku, Fukuoka 819-0395, Japan*

[g] *AIST-Kyushu University Hydrogen Materials Laboratory (HydroMate), 744 Motooka, Nishi-ku, Fukuoka 819-0395, Japan*

[h] *SINTEF Materials and Chemistry, PO Box 124 - Blindern, NO-0314 Oslo, Norway*

ABSTRACT

A new model for hydrogen-assisted fatigue crack growth (HAFCG) in BCC iron under a gaseous hydrogen environment has been established based on various methods of observation, i.e., electron backscatter diffraction (EBSD), electron channeling contrast imaging (ECCI) and transmission electron microscopy (TEM), to elucidate the precise mechanism of HAFCG. The FCG in gaseous hydrogen showed two distinguishing regimes corresponding to the

unaccelerated regime at a relatively low stress intensity factor range, ΔK, and the accelerated regime at a relatively high ΔK. The fracture surface in the unaccelerated regime was covered by ductile transgranular and intergranular features, while mainly quasi-cleavage features were observed in the accelerated regime. The EBSD and ECCI results demonstrated considerably lower amounts of plastic deformation, i.e., less plasticity, around the crack path in the accelerated regime. The TEM results confirmed that the dislocation structure immediately beneath the crack in the accelerated regime showed significantly lower development and that the fracture surface in the quasi-cleavage regions was parallel to the {100} plane. These observations suggest that the HAFCG in pure iron may be attributed to "less plasticity" rather than "localized plasticity" around the crack tip.

KEYWORDS

Fatigue, hydrogen embrittlement, dislocation structures, electron back-scattered diffraction (EBSD), transmission electron microscopy (TEM)

INTRODUCTION

Hydrogen has the potential to become one of the world's major energy carriers, particularly in automotive applications but also in other industries. However, technical obstacles are currently limiting the economic competitiveness against conventional sources such as fossil fuels or nuclear power. In particular, cheaper, hydrogen compatible, structural materials are necessary for further progress toward a hydrogen-energy-based society. Low-alloy and carbon steels with BCC lattice structures are the best contenders considering their price; however, the understanding of hydrogen effects on these types of steels is far from complete [1]. Specifically, fatigue crack growth (FCG) is one of the most important properties to ensure the reliability of materials in practical use [2].

For steels in corrosive environments, such as hydrogen gas or a sour atmosphere, hydrogen-induced enhancement of the FCG rate shows a strong dependence on the crack tip stress intensity, which is often interpreted as an interaction and/or superposition of the sustained load stress-corrosion cracking and pure mechanical fatigue [3,4]. In high-strength steels, the dominant mechanism of corrosion fatigue is determined by whether the stress intensity level is above or below the threshold stress intensity value for hydrogen-induced crack growth under a static load (K_{IH}) [5,6]. Based on the same argument, it was long believed that low or medium-strength steels are relatively immune to hydrogen embrittlement (HE) from fatigue, due to their high K_{IH} values measured in fracture toughness tests [7]. However, the FCG tests revealed that these materials can also be susceptible to HE even at stress intensity values much lower than K_{IH} [8,9]. The FCG data for low-strength steels also shows a two-stage behavior, which, in this article, we will refer to as Stage I for the unaccelerated regime at the stress intensity factor range (ΔK) lower than the critical stress intensity factor range for hydrogen-assisted FCG (HAFCG), ΔK^{T}, and Stage II for the accelerated regime for ΔK above ΔK^{T}. It should be noted that ΔK^{T} does not correspond to the measured K_{IH} values via monotonic fracture toughness tests.

While the hydrogen-assisted cracking in high-strength steels beyond K_{IH} is generally characterized by brittle intergranular fracture [4,10–12], in low or medium-strength steels subjected to HAFCG, the transgranular quasi-cleavage (QC) fracture accompanied by brittle-like striations on the fracture surfaces is frequently observed [13–19]. Based on the understanding that the QC fracture accompanied by brittle-like striations is the key to understand the underlying mechanism dominating the HAFCG in low-strength steels, numerous studies have been conducted to elucidate the formation mechanism of such fractographic features, and several models have been proposed [14,16,20–25]. These studies are based on the fundamental theories

for HE, such as hydrogen-enhanced decohesion (HEDE) [14,26,27], hydrogen-enhanced localization of plasticity (HELP) [15,28,29], hydrogen-enhanced stabilization of lattice defects [16,30], or their combinations. However, all of these previous models still lack direct and critical supporting evidence, especially from the perspective of crystallographic orientations of the fracture paths, the amount of plastic deformation around the crack tip, and the corresponding dislocation structures.

In this study, we conducted FCG tests of a commercially pure iron, which is a simplest representative system for BCC steels, in hydrogen gas at various pressures. To characterize the alteration of the crack tip microstructure evolution during the FCG tests at different length scales, multi-scale observations with optical microscopy (OM), scanning electron microscopy (SEM) and transmission electron microscopy (TEM) were performed to identify the fracture paths in the hydrogen gas. Even though most of the past studies have claimed the involvement of localized plasticity-mediated mechanisms in the crack propagation process, investigations in the present research successfully demonstrated the evidence of just the reduction, *i.e.*, not localization, of plastic strain around the crack propagation paths. This finding suggests that brittle-type cracking without extensive plasticity is crucial in causing the acceleration of FCG rather than the localized ductile fracture.

MATERIAL AND EXPERIMENTAL METHODS

A hot-rolled commercially pure iron plate (JIS-C2504) with the chemical composition of 0.001%C-0.07%Mn-0.010%P-0.003%S was used in this study. The yield stress, σ_Y, and tensile strength, σ_B, measured in air were 133 MPa and 252 MPa, respectively. The compact-tension (CT) specimens with a width, *W*, of 50.8 mm, and a thickness, *B*, of 10.0 mm were cut from the

longitudinal-transverse (L-T) orientation of the hot-rolled plate. The FCG tests were performed in laboratory air and hydrogen gas at pressures of 0.7 and 90 MPa at room temperature (RT), in accordance with the ASTM E647 [31] standard. A constant load range condition (ΔP-constant tests) was used to acquire the fatigue data (da/dN-ΔK curves) and fracture surfaces, while a constant ΔK condition (ΔK-constant tests) was chosen to examine the fracture surfaces and lateral fracture paths via SEM and TEM analyses. The ΔK values in the FCG tests were calculated according to the following equation [31]:

$$\Delta K = \frac{\Delta P(2+\alpha)}{B\sqrt{W}(1-\alpha)^{3/2}}(0.886 + 4.64\alpha - 13.32\alpha^2 + 14.72\alpha^3 - 5.6\alpha^4) \quad (1)$$

where α is the normalized crack length defined by a/W. The crack length, a, was monitored via the unloading elastic compliance method based on the following equations [31]:

$$\frac{a}{W} = 1.0010 - 4.6695u_x + 18.46u_x^2 - 236.82u_x^3 + 1214.9u_x^4 - 2143.6u_x^5 \quad (2)$$

$$u_x = \left(\left[\frac{EV_gB}{P}\right]^{1/2} + 1\right)^{-1} \quad (3)$$

where E is Young's modulus, V_g is the crack-mouth opening displacement (COD) and P is the applied load. The COD was measured using a clip-on gauge attached to the crack mouth of the CT specimens. A load ratio, R, of 0.1 was selected for all the FCG tests. In our previous work [15], it was confirmed that a significant acceleration of the FCG can be seen in low carbon steel tested in hydrogen gas at the testing frequency of 1 Hz. Therefore, the same frequency was chosen in this study. After the ΔP-constant tests, the side surfaces of the specimens were investigated using the OM. The specimens were then broken into two parts by additional fatigue loading in air, and the fracture surfaces were investigated using SEM operated at 15 kV. In contrast, the specimens subjected to ΔK-constant tests were cut along the mid-thickness section

and the surfaces were polished with colloidal SiO_2. A grain orientation analysis was performed along the fracture path using electron back-scattered diffraction (EBSD) with a beam step size of 1 μm and acceleration voltage of 15 kV. To analyze the plastic deformation around the fracture path, the grain reference orientation deviation (GROD) method was applied to the obtained crystal orientation maps. In the GROD analysis, the average crystal orientation of each grain was used as the orientation references, and the angular deviation from those references was mapped on each scanned point. A novel misorientation angle-dispersed plastic deformation distribution (MADPDD) technique was introduced to quantify the plastic deformation. This technique uses the raw data from the GROD maps to plot the number of pixels versus the misorientation angle, resulting in a MADPDD curve. This analysis is useful to compare the plastic deformation since it shows quantifiable differences between the samples tested in different atmospheres and can uncover subtle variations, which may not be directly visible from the GROD maps. A MATLAB script used for this analysis can be accessed at https://github.com/domasbi/MADPDD. Additionally, electron channeling contrast imaging (ECCI), which is a powerful tool to elucidate the deformation structure in bulk materials [32], was conducted for the same samples with an accelerating voltage of 30 kV. The TEM samples were directly extracted from the fracture surfaces of the Δ*K*-constant test specimens using a JEOL JIB-4500 focused ion beam (FIB) machine. A 2 μm thick carbon layer was deposited on the surfaces before the sample extraction to preserve the fracture surface features. The samples were observed using a FEI Titan G2, field-emission-TEM, operated at 300 kV in the high-angle annular dark-field (HAADF) scanning TEM (STEM) mode. In addition to the STEM observation, selected area electron diffraction patterns (SADP) were obtained using the conventional parallel beam TEM mode to analyze the crystallographic orientations of the fracture surface formed in hydrogen gas.

RESULTS

I. Fatigue crack growth curves

Fig. 1 illustrates the relationships between the FCG rate, da/dN, and the stress intensity factor range, ΔK, obtained via ΔP-constant tests in air and hydrogen gas.

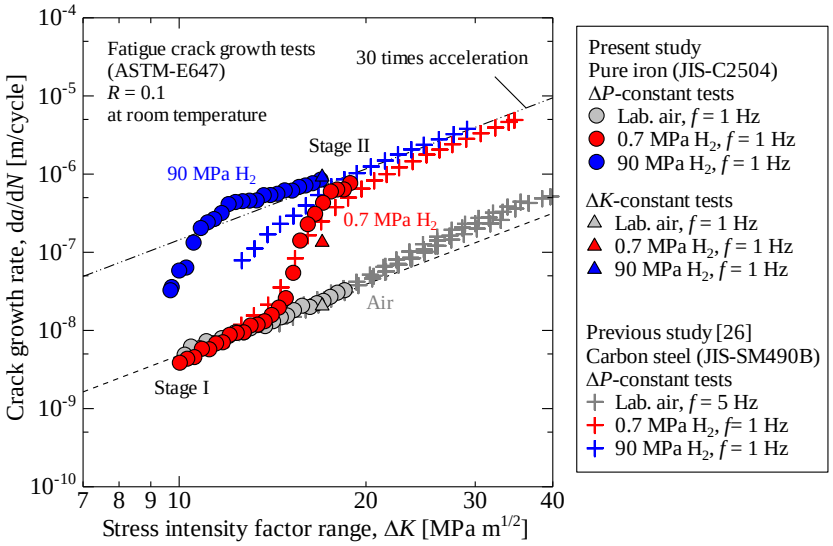

Fig. 1 The FCG curves of pure Fe (JIS-C2504) measured in laboratory air and hydrogen gas with pressures of 0.7 and 90 MPa at RT, together with the data of a low carbon steel (JIS-SM490B) in the same environmental conditions [15].

The crack growth curve was linear in a logarithmic scale for air throughout the tested ΔK range. However, in the case of hydrogen gas, a clear distinction was visible between Stage I (relatively low ΔK regime with no FCG acceleration) and Stage II (higher ΔK regime with significant FCG acceleration). The transition point between the two regimes was strongly affected by the hydrogen pressure. Namely, increasing the hydrogen pressure made the transitional stress intensity factor range, ΔK^{T}, from Stage I to II to shift to lower values. The effect of hydrogen was to enhance the crack growth rate in Stage II by a factor of 30 compared to the sample

fatigued in air. Furthermore, this effect was independent of the hydrogen pressure. To compare the FCG character of pure iron with other BCC steel, our previous data from a low carbon steel (JIS-SM490B) [15] obtained in the same environmental conditions are also plotted in the same diagram. A similar tendency is seen in the case of carbon steel, suggesting that the identical mechanism is responsible for the FCG acceleration in these two materials.

II. Fracture surfaces and deformation behavior on the lateral surface of CT specimens

Fig. 2 shows the fracture surfaces of the samples fatigued in air and those fatigued in 0.7 MPa and 90 MPa hydrogen gas. Ductile transgranular features with narrow ductile striations covered the entire fracture surface in the case of air. The spacing of these striations was more than one order of magnitude larger than the macroscopic FCG rate, which is a typical tendency for the low strength steels fatigued under relatively low stress intensity (ΔK = 10 ~ 20 MPa $m^{1/2}$) [25,33].

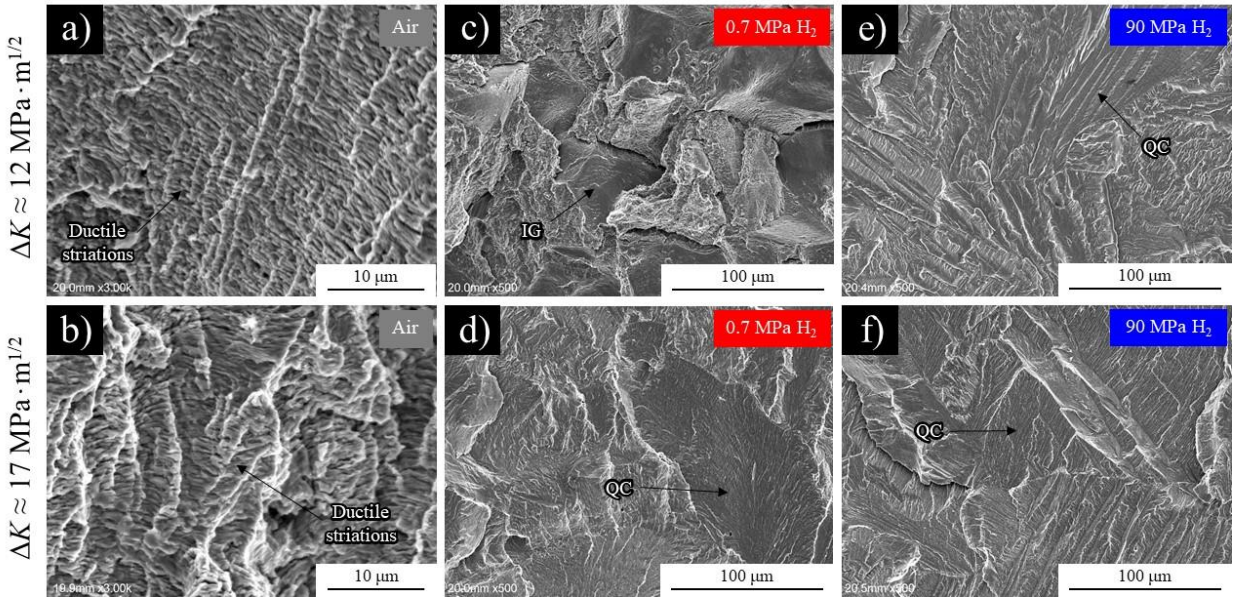

Fig. 2 SEM images of the fracture surfaces of the specimens subjected to ΔP-constant tests in a) and b) air, c) and d) 0.7 MPa H_2, and e) and f) 90 MPa H_2 at different ΔK values. The crack growth directions are from bottom to top.

On the other hand, the fracture surfaces formed in hydrogen gas exhibited a combination of ductile transgranular and intergranular (IG) fracture features in the Stage I regime and QC features decorated with brittle-like striations in the Stage II regime (Fig. 3). The IG fracture can be distinguished by relatively flat surfaces without any traces of the deformation processes. On the other hand, the QC fracture can be recognized by stepped surfaces decorated with river patterns, which are distinct features of this type of fracture. A similar transition from IG to QC fracturing between Stages I and II has also been reported in Armco iron [34] and some pipeline steels [18,35] tested in hydrogen gas. In contrast, Suresh and Ritchie studied the FCG behavior of several ferritic or martensitic low or medium strength steels in hydrogen gas, and concluded that the transition point of Stages I and II is determined from the threshold stress intensity needed to trigger the fracture along the grain boundaries [36].

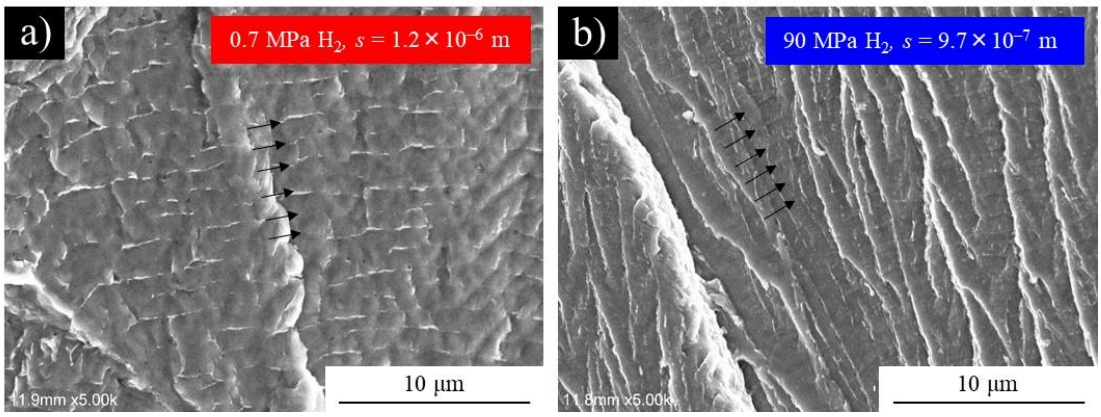

Fig. 3 SEM images of the brittle-like fatigue striations formed in a) 0.7 MPa H_2 and b) 90 MPa H_2 at $\Delta K \approx 17$ MPa·m$^{1/2}$ (Stage II), together with the average striation spacing, *s* in the insets. The crack growth directions are from bottom to top.

However, in this study, the results suggested the existence of a strong relationship between the formation of the QC fracture surface and FCG acceleration rate in hydrogen gas, whereas the IG

fracture had less of an impact on the macroscopic FCG rate. Therefore, we conclude that the beginning of Stage II is the starting point of the QC fracture rather than the IG fracture.

The QC is the most common fractographic feature resembling the hydrogen-related fracture in low strength materials, which has been frequently observed on specimens subjected to not only fatigue but also monotonic loading tests [37,38]. The technical term QC has been derived due to its appearance similar to cleavage, but it is generally interpreted that this type of fracture does not exactly follow along the known cleavage plane of the crystals [39]. The striation spacing on the QC coincided relatively well with the macroscopic FCG rate, as shown in Figs. 3 a) and b), indicating that these striations were formed on a cycle-by-cycle basis. Based on the observation of the reduced slip traces detected on the crack wake of the specimen lateral surfaces [24,40], Matsuoka et al. suggested that in carbon steels and low alloy steels, the formation of those QC features and corresponding FCG acceleration in hydrogen gas is a consequence of the localized plastic flow into the crack tip region. To validate the consistency of the results in pure iron with the aforementioned assertion, the surfaces of the CT specimens used in this study were also observed via OM. Fig. 4 shows optical micrographs of the area surrounding the crack tip in specimens fractured in air and hydrogen gas at the corresponding ΔK of approximately 17 MPa·m$^{1/2}$. The crack wake in air was decorated by features consistent with severe plastic deformation; however, a slight localization of the slip lines was detected in the 0.7 MPa hydrogen gas. Furthermore, the plastic deformation seemed to be highly localized near the fracture path, which was in good agreement with the results reported in previous studies [24,40].

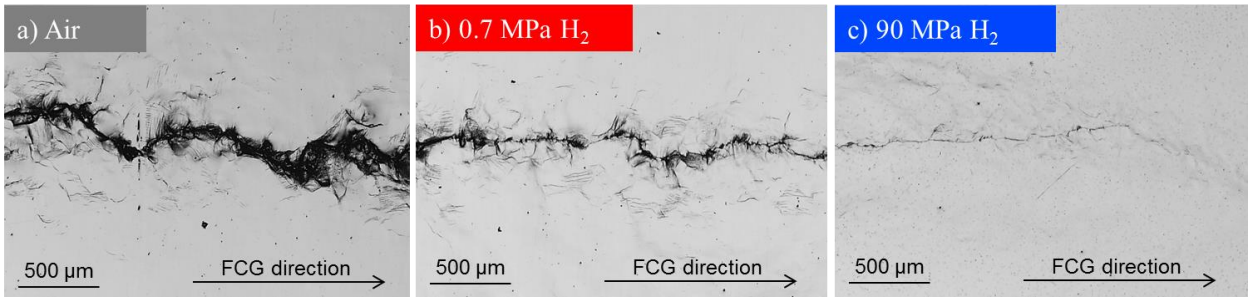

Fig. 4 Optical micrographs of the side surfaces of CT specimens after Δ*P*-constant tests in a) air, b) 0.7 MPa H_2 and c) 90 MPa H_2 in stage II ($\Delta K \approx 17$ MPa $m^{1/2}$).

III. Plasticity quantification using EBSD and ECCI

While the observation of the specimen surfaces around the fracture path (Fig. 4) showed a similar trend as reported by Matsuoka et al. [24,40], *i.e.*, the localization of plasticity in the vicinity of the crack tip in hydrogen gas, the strain analysis using EBSD revealed a completely different aspect. Fig. 5 shows the crystallographic orientation maps (Figs. 5 a) - c)) and corresponding GROD maps (Figs. 5 d) - f)) along the cracks that propagated in air and hydrogen gas in Δ*K*-constant tests at $\Delta K \approx 17$ MPa $m^{1/2}$. It is noted that the FCG rates in the Δ*K*-constant tests were similar to those in the Δ*P*-constant tests at the corresponding Δ*K* as plotted together in Fig. 1. While clear evidence of plastic deformation was seen along the crack formed in air (Fig. 5 d)), such plasticity expansion became extremely small in the 0.7 MPa hydrogen gas (Fig. 5 e)). Moreover, the crack in the 90 MPa hydrogen gas (Fig. 5 f)) showed almost no evidence of plasticity around the fracture path, indicating that the crack propagated in a brittle manner without extensive plasticity. The overview of the dislocation structures in the regions marked with black dashed lines in Figs. 5 a) - c) revealed with the ECCI technique is shown in Figs. 6 a) - c). A heavy plastic deformation caused the formation of fine sub-grain-like features just around the crack path in the specimen fatigued in air (Fig. 6 a)). In contrast, the sample fatigued in the

0.7 MPa hydrogen gas demonstrated a much cleaner microstructure with only a few regions where a deformed structure is visible (Fig. 6 b)). Following the same trend, the sample fatigued in the 90 MPa hydrogen gas showed a nearly undeformed microstructure around the crack path, indicating heavily suppressed plastic deformation (Fig. 6 c)). Additionally, whereas the crack propagation path in air was wavy, some parts of the paths in hydrogen gas were completely straight through one crystal grain, as indicated with the yellow arrowheads in Fig. 6 b) and c). These yellow dashed lines indicate the traces of the {100} crystal planes determined from the EBSD analysis on the same area (Figs. 5 a) - c)). The straight crack paths in the hydrogen gas were exactly parallel to the traces of the {100} plane, which is the cleavage plane of the BCC crystals, implying that the brittle-type fracture due to the cleavage process was the main reason for the aforementioned reduction of the crack tip plasticity.

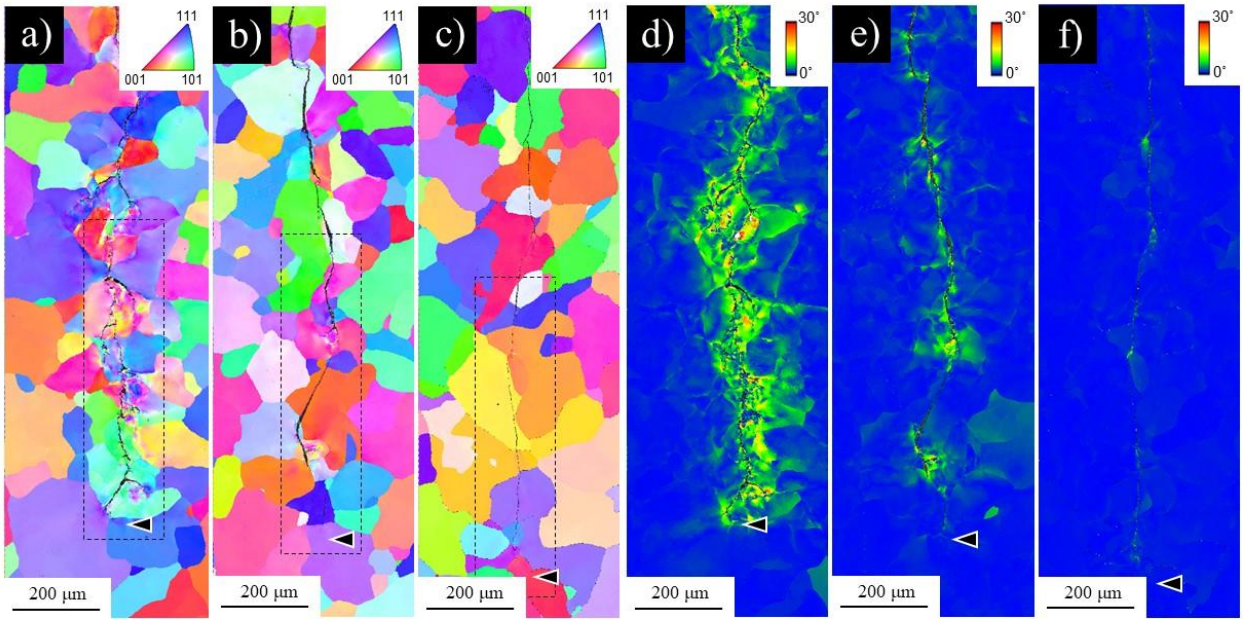

Fig. 5 Crystallographic orientation maps and corresponding GROD maps around the mid-thickness fracture paths in a) and d) air, b) and e) 0.7 MPa H_2, and c) and f) 90 MPa H_2 acquired with a beam step size of 1.0 µm. The arrowheads indicate the crack tip positions.

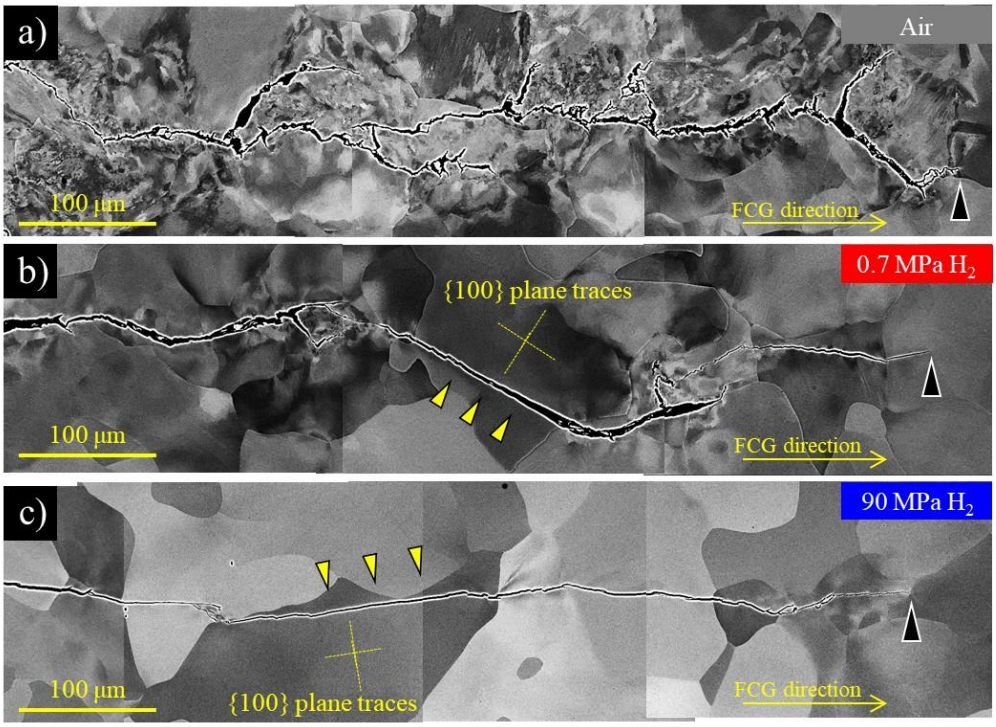

Fig. 6 ECC images around the mid-thickness fracture paths in a) air, b) 0.7 MPa H_2 and c) 90 MPa H_2. The captured areas correspond to the regions surrounded with black dashed lines in Figs. 5 a) - c). The black arrowheads indicate crack tip positions, while the yellow arrowheads show the fracture path along the cleavage plane.

The MADPDD graph in Fig. 7 shows the distribution of all the pixels in the GROD maps (Figs. 5 d) - f)) in accordance to which misorientation angles they correspond to, providing a tool to analyze the amount of plastic deformation in a more quantitative way. For example, in the Stage II regime, plastic deformation was drastically reduced in the case of hydrogen gas (Figs. 5 e) and f)), which was emphasized from the MADPDD analysis based on the GROD maps. For the case of the 0.7 MPa hydrogen gas (red line in Fig. 7), the total number of pixels displaying a misorientation was significantly lower than that observed for the sample fatigued in air (gray line in Fig. 7). The maximum misorientation observed was approximately 35˚ for the 0.7 MPa

hydrogen gas, while the maximum misorientation was above 40˚ for air. In addition, the blue line corresponding to the sample fatigued in the 90 MPa hydrogen gas showed an even lower misorientation and terminated at an angle of approximately 17˚. This further indicates that much less plasticity was involved and the lower magnitude plastic strain was needed for the material to fail in the case of hydrogen gas. This effect became stronger at the higher hydrogen gas pressure.

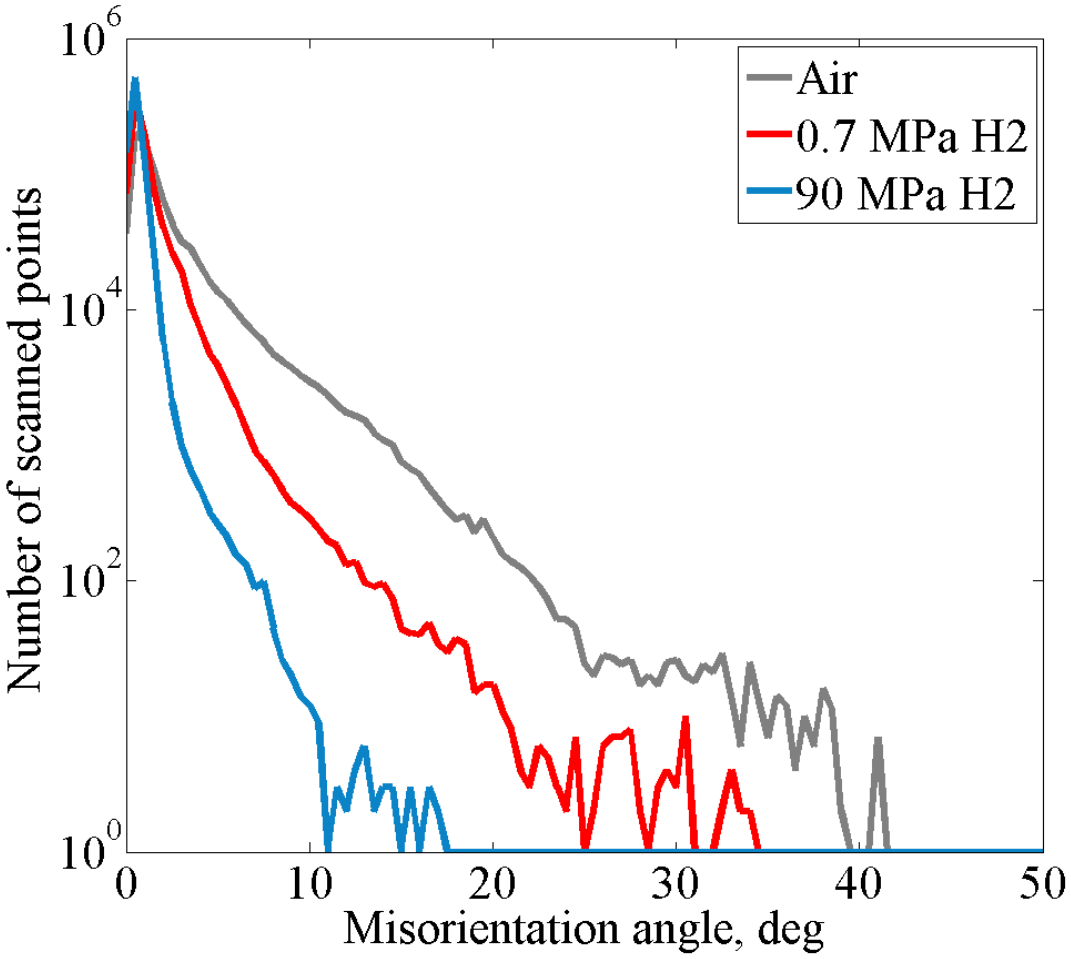

Fig. 7 Misorientation angle dispersed plastic deformation distribution (MADPDD) graph obtained from the GROD maps indicated in Figs. 5 d) - f).

IV. Dislocation structures characterized by TEM

Thin-foil samples for TEM were directly extracted from the ductile striations formed in air and from brittle-like striations formed in hydrogen gas using FIB. The dislocation structure immediately beneath the fracture surfaces were examined by STEM observation as indicated in Fig. 8. Dislocation cells were seen to dominate the dislocation structure in the sample fatigued in air (Fig. 8 a)) with a uniform cell size distribution. However, below the quasi-cleavage fracture surface formed in the hydrogen gas (Figs. 8 b) and c)), only dislocation tangles and individual dislocations were observed. It is important to note that the amount of dislocations in Figs. 8 b) and c) depends on the sample thickness, which was difficult to control during the sample preparation process. In this specific case, the specimen fatigued in the 0.7 MPa hydrogen gas was approximately 160 nm thick, and the one fatigued in the 90 MPa hydrogen gas was approximately 250 nm thick as measured using electron energy loss spectroscopy (EELS). The difference in the thickness between the two samples complicated the comparison of plasticity. In addition, the calculation of the dislocation densities was difficult due to their high concentration at the dislocation tangles. Nevertheless, the obvious difference between specimens fatigued in air and hydrogen gas demonstrated a significant reduction of plasticity. The diffraction patterns in the insets of the corresponding images showed that the orientations of the fracture surfaces were very close to the {100} type cleavage plane, both in the 0.7 and 90 MPa hydrogen gases, which can reinforce the discussion about the cleavage type fracture that was responsible for the reduction of plasticity and corresponding FCG acceleration, as shown in Fig. 6.

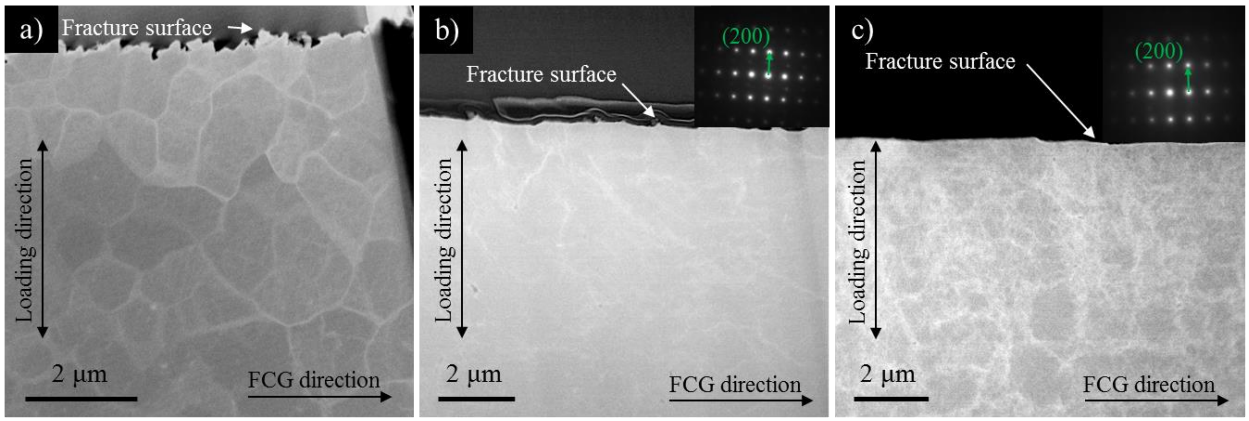

Air | 0.7 MPa H_2, ΔK=17 MPa·m$^{1/2}$ | 90 MPa H_2, ΔK=17 MPa·m$^{1/2}$

Fig. 8 Dislocation structures immediately beneath the fracture surfaces of the samples fatigued in a) air, b) 0.7 MPa H_2, and c) 90 MPa H_2. The SADPs acquired from the [011] zone axis are indicated in the insets.

DISCUSSION

Based on our experimental FCG data and fracture surface results, we can determine that the emergence of the QC features on the fracture surface (Fig. 2) coincides well with the transition from the Stage I to Stage II regimes. We also observed that the fraction of the QC features reaches close to 100% surface coverage at the point where the transition ends, indicating that this type of fracture had a critical influence on the acceleration of the FCG. Additionally, the increase in the hydrogen pressure did not have any influence on the FCG acceleration enhancement in the stage II regime. This means that the maximum amount of FCG acceleration enhancement was controlled by the coverage of the QC fracture, and as it reaches 100% there is no further enhancement by increasing the hydrogen pressures. On the other hand, higher hydrogen pressures caused a shift of the ΔK^T to lower values, showing that higher hydrogen

concentration around the crack tip region decreases the critical stress intensity needed to trigger the QC type fracture.

The plastic deformation analysis from the EBSD revealed that the maximum misorientation values within the grains are much lower in the hydrogen gas than in air. This indicates that the plastic deformation is suppressed but not localized as reported elsewhere [41,42]. It is known that misorientation analyses via EBSD, such as the kernel average misorientation (KAM), grain orientation spread (GOS) or GROD, qualitatively reflect the plastic strain inside the material and corresponding density of the geometrically necessary dislocations (GNDs) [43–45]. Therefore, the smaller GROD value clarifies the fact that lower plastic strain amplitude is needed for pure Fe to fracture when the specimen is exposed to higher pressures of hydrogen. To complement these findings, we provide micrographs of the dislocation structures acquired using ECCI and STEM techniques in Fig. 6 and Fig. 8. According to past studies [46–48], dislocation evolution is directly linked to the magnitude of the plastic strain applied to the material. At the initial stages, individual dislocations and dislocation tangles are formed, and further plastic deformation forces the dislocations to agglomerate into veins, walls and finally cell structures. Applying these findings to our work, we deduce that specimens fatigued in air sustained a high plastic strain, while only slightly developed structures, even very close to the fracture surfaces (Figs. 8 b) and c)) in hydrogen, illustrated an example of material failure at lower plastic strains (less plasticity). In addition, the EBSD maps and SADPs acquired from TEM clarified the fracture along the {100} cleavage planes, providing a new finding to interpret the formation mechanism of QC during hydrogen-related fatigue in pure iron. These results support the statement that hydrogen promoted the cleavage fracture. The decisive mechanism for

this fracture is discussed below in terms of the hydrogen-induced reduction of dislocation motion in the BCC crystal under critical stress intensity and hydrogen concentration.

According to works by Caillard [49,50] and Matsui et al. [51–53] different alloying elements, including hydrogen, can both soften and harden pure Fe by affecting the motion of screw dislocations. This effect depends on many factors, such as temperature, strain rate, and material purity. Matsui et al. [52] deduced that the softening occurs due to hydrogen enhancing the nucleation of kink pairs and increasing the mobility of screw dislocations. On the other hand, at higher hydrogen concentrations, the hydrogen may form pairs or clusters or interact with interstitial carbon atoms and pin the edge dislocations. This can cause a significant reduction of the screw dislocation mobility by slowing down the kinked edge components of the screws. Based on these hypotheses, we assume that the cleavage fracture in the Stage II regime is triggered from a reduction of the screw dislocation motion, *i.e.,* hindering the plastic relaxation, which is induced by a combination of the high stress and hydrogen concentrations. On the other hand, due to the lower stress intensity in the Stage I regime the screw dislocations become more mobile, which reduced or eliminated the pinning effect, resulting in softening due to the hydrogen. Such a phenomenon was also confirmed in the atomistic calculations by Taketomi et al. [54]. Specifically, in the crack tip zone, the role of the tensile stress is not only to trigger the fracture but also to dilate the lattice, which attains a higher hydrogen concentration in the vicinity of the crack tip to operate dislocation locking and weakening of the matrix bonding.

Another important topic of this work is the formation of the brittle-striations. In non-aggressive environments such as ambient air or vacuum, the fatigue striations in ductile materials are believed to be formed by the normal slip-off and reverse slip processes, as was proposed by Bichler and Pippan [55] (Fig. 9 a)). On the other hand, in hydrogen gas or hydrogen pre-charged

conditions, hydrogen atoms can concentrate around the crack tip due to the penetration from newly created bare surfaces or stress-induced diffusion. According to the hydrogen enhanced successive fatigue crack growth (HESFCG) model proposed by Matsuoka et al. [24], these localized hydrogen atoms enhance the dislocation motion, thereby causing localized plastic flow and less crack tip blunting. Additionally, there is only a minimal reverse-slip in the unloading process because of the small extent of the plasticity around the crack tip, which blurs the striation borders. The schematics of the HESFCG model are illustrated in Fig. 9 b).

In contrast, a study by Marrow et al. [14] concluded that the brittle-like striations observed on a ferritic stainless steel tested in atmospheric pressure hydrogen gas are the consequence of the local cleavage process in each loading cycle as indicated in Fig. 9 c). When the specimen is loaded in hydrogen gas, the dislocations are emitted from the crack tip through alternating slip process and the crack tip is blunted. A zone with a maximum hydrostatic stress and high dislocation density is created ahead of the crack tip. Therefore, the hydrogen diffuses toward the crack tip and becomes trapped in that zone. The combination of the high local stress and high hydrogen concentration causes the reduction in the lattice cohesive energy [27,56], and results in a cleavage fracture.

Another model for brittle striation formation has been proposed by Nishikawa et al. [16]. According to their model, the brittle striation formation in low carbon steel fatigued in air and hydrogen consists of three subsequent processes: i) crack tip opening; ii) microscopic defect nucleation ahead of the crack tip due to hydrogen-enhanced stabilization of point defects [30,57]; and iii) final crack growth by a coalescence of the main crack with the primary defects due to ductile tearing (Fig. 9 d)). However, they did not show direct evidence of such microvoid formation ahead of the crack tip. Additionally, our findings of the underdeveloped dislocation

structures and relatively flat fracture surface parallel to the {100} cleavage plane between the striations contradict this model.

In the context of the aforementioned experimental evidences, we propose the following sequence for the brittle striation formation model, as illustrated in Fig. 9 e): i) as the loading cycle starts, the crack tip is blunted with an alternating slip mechanism and dislocation emission from the crack tip; ii) a maximum hydrostatic stress field is created just ahead of the main crack tip [58], which acts as a lower chemical potential zone for preferential hydrogen agglomeration; iii) the combination of the critical tensile stress and critical hydrogen concentration causes suppressed plastic deformation and a primary cleavage micro crack formation ahead of the crack tip; and iv) the main crack and the primary cleavage micro-crack coalesce and propel the main crack forward until it is arrested. This mechanism is similar to Marrow's model from the viewpoint that the crack growth process is assumed as a cleavage. However, we believe that the reduction of the screw dislocation mobility plays a major role in inducing a cleavage fracture as opposed to Marrow's statement that trapped hydrogen induces cleavage by reducing bonding energy between the matrix atoms.

According to existing research the brittle striations on the QC fracture surface during the fatigue experiments are formed on a cycle-by-cycle basis, as was experimentally confirmed in some conventional BCC steels [16,40]. Even in pure iron, we found a good coincidence between the striation spacing and the FCG rate (Fig. 3). This fact demonstrates that the macroscopic behavior of HAFCG in BCC iron is still controlled in a stable manner, even though the fracture event is microscopically catastrophic, *i.e*., cleavage. Currently, the reason for this strong contradiction remains unclear, and further investigation that can link the micro-scale fracture phenomena to macro-scale crack propagation behavior is required. It is also important to

evaluate the applicability of our assertion to other conventional materials and some influencing factors controlling HAFCG, such as the loading frequency [16,18] or testing temperature [14]. These will be the subjects of further studies.

Finally, an important feature of our work is the stress state of the observed regions. Samples used in our observation were taken from the mid-thickness part of the specimens with a plane-strain state that dominates the macroscopic FCG rate. In comparison to the plane-stress state, the plane-strain state causes higher lattice dilatation, which can facilitate a hydrogen induced cleavage fracture. It is important to note that in contrast to the present study, some other works were based on the observations of the lateral surface of specimens with a plane-stress state, which could lead to different findings from ours [15,24]. Therefore, at the end of this paper, the authors point out that the use of the mid-thickness sample rather than the surface sample is necessary in attempting to understand the dominating mechanism of HAFCG.

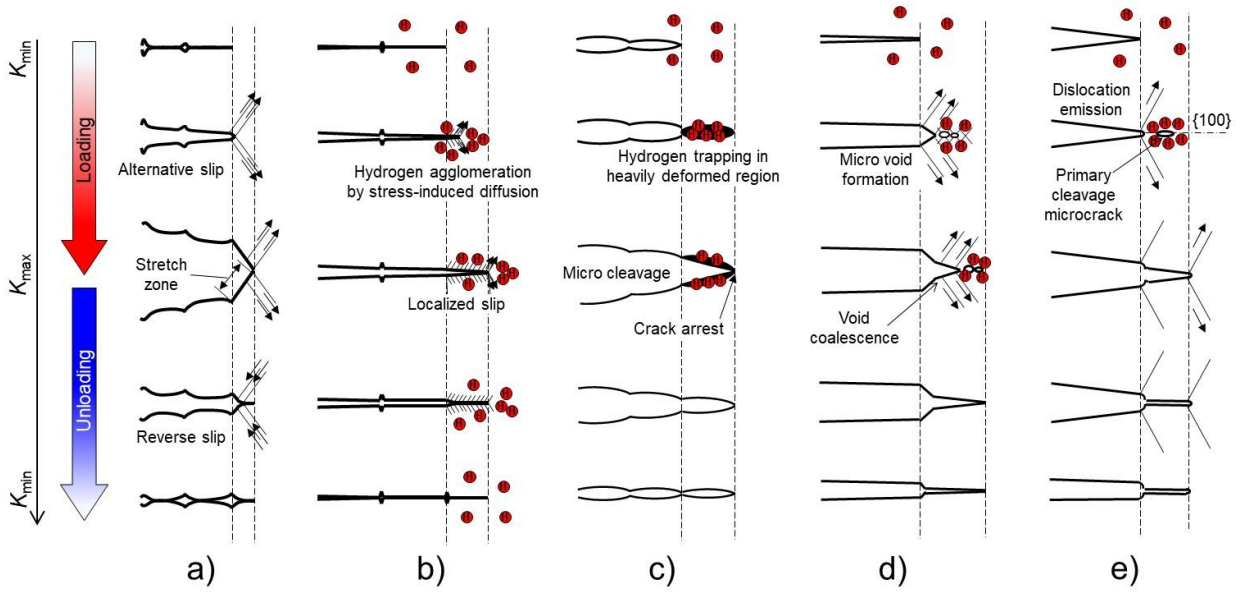

Fig. 9 Ductile fatigue striation formation model a) in air, and brittle-like striation formation models b) - e) under the influence of hydrogen: b) HESFCG model proposed by Matsuoka; c) cleavage-like model proposed by Marrow; d) ductile tearing model proposed by Nishikawa; and e) present model based on the less plasticity mechanism.

CONCLUSIONS

1. Hydrogen gas environments enhanced the fatigue crack growth (FCG) acceleration in pure iron by ~30 times above the critical stress intensity factor range, ΔK^{T}. The ΔK^{T} value was directly affected by the hydrogen pressure, *i.e.*, increasing pressure significantly decreased the starting point for the FCG acceleration. However, the FCG acceleration rate was almost independent of the hydrogen gas pressure beyond ΔK^{T}.
2. The significant FCG acceleration beyond ΔK^{T} was accompanied by the formation of hydrogen induced quasi-cleavage fracture. Additionally, below ΔK^{T}, hydrogen also altered the fractographic features from the ductile striations to the brittle appearance intergranular facets. However, those IG had a much lesser deleterious effect on the macroscopic FCG rate than the QC type fracture.

3. Plastic deformation analyses on the mid-thickness facture paths revealed that the dislocation structure evolution, *i.e.*, cells or sub-grain formation around the crack was dramatically reduced under the presence of hydrogen, when the fracture was characterized by quasi-cleavage features. This fact implies that the brittle type fracture mechanism (less plasticity) has a crucial role in triggering hydrogen-assisted FCG in BCC iron.

4. Dislocation structures immediately beneath the fracture surface acquired by TEM revealed a low level of plasticity in hydrogen gas compared with those in air. In addition, electron diffraction patterns showed that the fracture in hydrogen gas was along the {100} crystal planes, implying that the hydrogen-induced cleavage cracking was the main contributor to the hydrogen-assisted FCG accompanying the significantly reduced plasticity.

ACKNOWLEDGEMENTS

This work was supported by JSPS KAKENHI Grant Numbers 16H04238 and 16J02960. The Research Council of Norway is acknowledged for its support through the Norwegian Center for Transmission Electron Microscopy, NORTEM (197405/F50). This study also forms part of the "HIPP" project from the PETROMAKS2 program, funded by the Research Council of Norway [Grant Number: 102006899].

BIBLIOGRAPHY

[1] M. Dadfarnia, A. Nagao, S. Wang, M.L. Martin, B.P. Somerday, P. Sofronis, Recent advances on hydrogen embrittlement of structural materials, Int. J. Fract. 196 (2015) 223–243. doi:10.1007/s10704-015-0068-4.

[2] ASME boiler and pressure vessel code. Section VIII, Rules for construction of pressure vessels. Division 2. New York, NY. American Society of Mechanical Engineers, (2007).

[3] I.M. Austen, P. Mcintyre, Corrosion fatigue of high-strength steel in low-pressure

hydrogen gas, Met. Sci. 13 (1979) 420–428. doi:10.1179/msc.1979.13.7.420.

[4] R.P. Wei, D. Landes, Correlation between sustained-load and fatigue crack growth in high strength steels for aggressive environment effects, Mater. Res. Stand. 12 (1972) 45–56.

[5] J.M. Barsom, Corrosion-fatigue crack propagation below KIscc, Eng. Fract. Mech. 3 (1971) 15–25. doi:https://doi.org/10.1016/0013-7944(71)90048-8.

[6] C.S. Kortovich, E.A. Steigerwald, A comparison of hydrogen embrittlement and stress corrosion cracking in high-strength steels, Eng. Fract. Mech. 4 (1972) 637–651. doi:10.1016/0013-7944(72)90004-5.

[7] K.A. Nibur, B.P. Somerday, C.S. Marchi, J.W. Foulk, M. Dadfarnia, P. Sofronis, The Relationship Between Crack-Tip Strain and Subcritical Cracking Thresholds for Steels in High-Pressure Hydrogen Gas, Metall. Mater. Trans. A. 44 (2012) 248–269. doi:10.1007/s11661-012-1400-5.

[8] P. Smith, A.T. Stewart, Effect of aqueous and hydrogen environments on fatigue crack growth in 2Ni-Cr-Mo-V rotor steel, Met. Sci. 13 (1979) 429–435. doi:http://dx.doi.org/10.1179/msc.1979.13.7.429.

[9] R.J. Walter, W.T. Chandler, Cyclic-load crack growth in ASME SA-105 grade II steel in high-pressure hydrogen at ambient temperature, in: A.W. Thompson, I.M. Bernstein (Eds.), Eff. Hydrog. Behav. Mater., 1976: pp. 273–286.

[10] P. Novak, R. Yuan, B.P. Somerday, P. Sofronis, R.O. Ritchie, A statistical, physical-based, micro-mechanical model of hydrogen-induced intergranular fracture in steel, J. Mech. Phys. Solids. 58 (2010) 206–226. doi:10.1016/j.jmps.2009.10.005.

[11] C. J. McMahon, Hydrogen-induced intergranular fracture of steels, Eng. Fract. Mech. 68 (2001) 773–788. doi:http://dx.doi.org/10.1016/S0013-7944(00)00124-7.

[12] J. Yamabe, T. Matsumoto, S. Matsuoka, Y. Murakami, A new mechanism in hydrogen-enhanced fatigue crack growth behavior of a 1900-MPa-class high-strength steel, Int. J. Fract. 177 (2012) 141–162. doi:10.1007/s10704-012-9760-9.

[13] H.J. Cialone, J.H. Holbrook, Effects of gaseous hydrogen on fatigue crack growth in pipeline steel, Metall. Trans. A. 16 (1985) 115–122. doi:10.1007/BF02656719.

[14] T.J. Marrow, P.J. Cotterill, J.E. King, Temperature effects on the mechanism of time independent hydrogen assisted fatigue crack propagation in steels, Acta Metall. Mater. 40 (1992) 2059–2068. doi:10.1016/0956-7151(92)90192-H.

[15] J. Yamabe, M. Yoshikawa, H. Matsunaga, S. Matsuoka, Hydrogen trapping and fatigue crack growth property of low-carbon steel in hydrogen-gas environment, Int. J. Fatigue. 102 (2017) 202–213. doi:10.1016/j.ijfatigue.2017.04.010.

[16] H. Nishikawa, Y. Oda, H. Noguchi, Investigation of the mechanism for brittle-striation formation in low carbon steel fatigued in hydrogen gas, J. Solid Mech. Mater. Eng. 5 (2011) 370–385. doi:10.1299/jmmp.5.370.

[17] Y. Ogawa, H. Matsunaga, J. Yamabe, M. Yoshikawa, S. Matsuoka, Unified evaluation of hydrogen-induced crack growth in fatigue tests and fracture toughness tests of a carbon steel, Int. J. Fatigue. 103 (2017) 223–233. doi:10.1016/j.ijfatigue.2017.06.006.

[18] B.P. Somerday, P. Sofronis, K.A. Nibur, C. San Marchi, R. Kirchheim, Elucidating the variables affecting accelerated fatigue crack growth of steels in hydrogen gas with low

oxygen concentrations, Acta Mater. 61 (2013) 6153–6170. doi:10.1016/j.actamat.2013.07.001.

[19] Y. Onishi, M. Koyama, D. Sasaki, H. Noguchi, Characteristic Fatigue Crack Growth Behavior of Low Carbon Steel under Low-pressure Hydrogen Gas Atmosphere in an Ultra-low Frequency, ISIJ Int. 56 (2016) 855–860. doi:10.2355/isijinternational.ISIJINT-2015-647.

[20] H. Nishikawa, Y. Oda, H. Noguchi, Loading-frequency effects on fatigue crack growth behavior of a low carbon steel JIS S10C in hydrogen gas environment, J. Solid Mech. Mater. Eng. 5 (2011) 104–116. doi:10.1299/jmmp.5.104.

[21] Y. Takahashi, M. Tanaka, K. Higashida, K. Yamaguchi, H. Noguchi, An intrinsic effect of hydrogen on cyclic slip deformation around a {110} fatigue crack in Fe-3.2wt.% Si alloy, Acta Mater. 58 (2010) 1972–1981. doi:10.1016/j.actamat.2009.11.040.

[22] S. Lynch, Hydrogen embrittlement phenomena and mechanisms, Corros. Rev. 30 (2012). doi:10.1515/corrrev-2012-0502.

[23] S.P. Lynch, Mechanisms of Fatigue and Environmentally Assisted Fatigue, ASTM STP675-EB. (1979) 174–213. doi:10.1520/STP35890S.

[24] S. Matsuoka, H. Tanaka, N. Homma, Y. Murakami, Influence of hydrogen and frequency on fatigue crack growth behavior of Cr-Mo steel, Int. J. Fract. 168 (2011) 101–112. doi:10.1007/s10704-010-9560-z.

[25] S. Lynch, Some fractographic contributions to understanding fatigue crack growth, Int. J. Fatigue. 104 (2017) 12–26. doi:10.1016/j.ijfatigue.2017.06.036.

[26] R.A. Oriani, Hydrogen Embrittlement of Steels, Annu. Rev. Mater. Sci. 8 (1978) 327–357. doi:10.1146/annurev.ms.08.080178.001551.

[27] A.R. Troiano, The role of hydrogen and other interstitials in the mechanical behavior of metals, Trans. ASME. 52 (1960) 54–80.

[28] C.D. Beachem, A new model for hydrogen-assisted cracking (hydrogen "embrittlement"), Metall. Trans. 3 (1972) 441–455. doi:10.1007/BF02642048.

[29] H.K. Birnbaum, P. Sofronis, Hydrogen-enhanced localized plasticity-a mechanism for hydrogen-related fracture, Mater. Sci. Eng. A. 176 (1994) 191–202. doi:10.1016/0921-5093(94)90975-X.

[30] M. Nagumo, Function of Hydrogen in Embrittlement of High-strength Steels, ISIJ Int. 41 (2001) 590–598. doi:http://doi.org/10.2355/isijinternational.41.590.

[31] ASTM E647-15e1, Standard Test Method for Measurement of Fatigue Crack Growth Rates, ASTM International, West Conshohocken, PA, 2015. www.astm.org.

[32] S. Zaefferer, N.N. Elhami, Theory and application of electron channelling contrast imaging under controlled diffraction conditions, Acta Mater. 75 (2014) 20–50. doi:10.1016/j.actamat.2014.04.018.

[33] H. Cai, A.J. McEvily, On striations and fatigue crack growth in 1018 steel, Mater. Sci. Eng. A. 314 (2001) 86–89. doi:10.1016/s0921-5093(00)01925-0.

[34] G. Bilotta, M. Arzaghi, G. Hénaff, G. Benoit, D. Halm, Hydrogen Induced Intergranular Failure in Armco Iron Under Fatigue Crack Propagation, in: Vol. 6B Mater. Fabr., ASME, 2016: p. V06BT06A026. doi:10.1115/PVP2016-63338.

[35] R.L. Amaro, N. Rustagi, K.O. Findley, E.S. Drexler, A.J. Slifka, Modeling the fatigue crack growth of X100 pipeline steel in gaseous hydrogen, Int. J. Fatigue. 59 (2014) 262–271. doi:10.1016/j.ijfatigue.2013.08.010.

[36] S. Suresh, R.O. Ritchie, Mechanistic dissimilarities between environmentally influenced fatigue-crack propagation at near-threshold and higher growth rates in lower strength steels, Met. Sci. 16 (1982) 529–538. doi:10.1179/msc.1982.16.11.529.

[37] T. Michler, J. Naumann, Microstructural aspects upon hydrogen environment embrittlement of various bcc steels, Int. J. Hydrogen Energy. (2010). doi:10.1016/j.ijhydene.2009.10.092.

[38] H. Matsunaga, M. Yoshikawa, R. Kondo, J. Yamabe, S. Matsuoka, Slow strain rate tensile and fatigue properties of Cr-Mo and carbon steels in a 115 MPa hydrogen gas atmosphere, Int. J. Hydrogen Energy. (2015). doi:10.1016/j.ijhydene.2015.02.098.

[39] M.L. Martin, J.A. Fenske, G.S. Liu, P. Sofronis, I.M. Robertson, On the formation and nature of quasi-cleavage fracture surfaces in hydrogen embrittled steels, Acta Mater. 59 (2011) 1601–1606. doi:10.1016/j.actamat.2010.11.024.

[40] M. Yoshikawa, T. Matsuo, N. Tsutsumi, H. Matsunaga, S. Matsuoka, Effects of hydrogen gas pressure and test frequency on fatigue crack growth properties of low carbon steel in 0.1-90 MPa hydrogen gas, Trans. JSME (in Japanese). 80 (2014) SMM0254-SMM0254. doi:10.1299/transjsme.2014smm0254.

[41] T. Hajilou, Y. Deng, B.R. Rogne, N. Kheradmand, A. Barnoush, In situ electrochemical microcantilever bending test: A new insight into hydrogen enhanced cracking, Scr. Mater.

132 (2017) 17–21. doi:10.1016/j.scriptamat.2017.01.019.

[42] Y. Ogawa, D. Birenis, H. Matsunaga, A. Thøgersen, Ø. Prytz, O. Takakuwa, J. Yamabe, Multi-scale observation of hydrogen-induced, localized plastic deformation in fatigue-crack propagation in a pure iron, Scr. Mater. 140 (2017). doi:10.1016/j.scriptamat.2017.06.037.

[43] S.I. Wright, M.M. Nowell, D.P. Field, A Review of Strain Analysis Using Electron Backscatter Diffraction, Microsc. Microanal. 17 (2011) 316–329. doi:10.1017/S1431927611000055.

[44] M. Calcagnotto, D. Ponge, E. Demir, D. Raabe, Orientation gradients and geometrically necessary dislocations in ultrafine grained dual-phase steels studied by 2D and 3D EBSD, Mater. Sci. Eng. A. 527 (2010) 2738–2746. doi:10.1016/j.msea.2010.01.004.

[45] C. Moussa, M. Bernacki, R. Besnard, N. Bozzolo, Statistical analysis of dislocations and dislocation boundaries from EBSD data, Ultramicroscopy. 179 (2017) 63–72. doi:10.1016/j.ultramic.2017.04.005.

[46] H. Mughrabi, K. Herz, X. Stark, Cyclic deformation and fatigue behaviour of alpha-iron mono-and polycrystals, Int. J. Fract. 17 (1981) 193–220. doi:10.1007/BF00053520.

[47] M.S. Pham, S.R. Holdsworth, Evolution of Relationships Between Dislocation Microstructures and Internal Stresses of AISI 316L During Cyclic Loading at 293 K and 573 K (20°C and 300°C), Metall. Mater. Trans. A. 45 (2013) 738–751. doi:10.1007/s11661-013-1981-7.

[48] J. Polák, Fatigue of Steels, Elsevier B.V., 2007. doi:http://dx.doi.org/10.1016/B978-

008043749-1/00312-7.

[49] D. Caillard, A TEM in situ study of alloying effects in iron. i - Solid solution softening caused by low concentrations of Ni, Si and Cr, Acta Mater. 61 (2013) 2793–2807. doi:10.1016/j.actamat.2013.01.048.

[50] D. Caillard, A TEM in situ study of alloying effects in iron. II - Solid solution hardening caused by high concentrations of Si and Cr, Acta Mater. 61 (2013) 2808–2827. doi:10.1016/j.actamat.2013.01.049.

[51] S. Moriya, H. Matsui, H. Kimura, The effect of hydrogen on the mechanical properties of high purity iron II. Effect of quenched-in hydrogen below room temperature, Mater. Sci. Eng. 40 (1979) 217–225. doi:10.1016/0025-5416(79)90192-7.

[52] H. Matsui, H. Kimura, S. Moriya, The effect of hydrogen on the mechanical properties of high purity iron I. Softening and hardening of high purity iron by hydrogen charging during tensile deformation, Mater. Sci. Eng. 40 (1979) 207–216. doi:10.1016/0025-5416(79)90191-5.

[53] H. Matsui, H. Kimura, A. Kimura, The effect of hydrogen on the mechanical properties of high purity iron III. The dependence of softening in specimen size and charging current density, Mater. Sci. Eng. 40 (1979) 227–234. doi:10.1016/0025-5416(79)90193-9.

[54] S. Taketomi, R. Matsumoto, N. Miyazaki, Atomistic study of the competitive relationship between edge dislocation motion and hydrogen diffusion in alpha iron, J. Mater. Res. 26 (2011) 1269–1278. doi:10.1557/jmr.2011.106.

[55] R. Pippan, C. Zelger, E. Gach, C. Bichler, H. Weinhandl, On the mechanism of fatigue

crack propagation in ductile metallic materials, Fatigue Fract. Eng. Mater. Struct. (2011). doi:10.1111/j.1460-2695.2010.01484.x.

[56] R.A. Oriani, P.H. Josephic, Testing of the decohesion theory of hydrogen-induced crack propagation, Scr. Metall. 6 (1972) 681–688. doi:10.1016/0036-9748(72)90126-3.

[57] K. Takai, H. Shoda, H. Suzuki, M. Nagumo, Lattice defects dominating hydrogen-related failure of metals, Acta Mater. 56 (2008) 5158–5167. doi:http://dx.doi.org/10.1016/j.actamat.2008.06.031.

[58] M.-J. Lii, X.-F. Chen, Y. Katz, W.W. Gerberich, Dislocation modeling and acoustic emission observation of alternating ductile/brittle events in Fe-3wt%Si crystals, Acta Metall. Mater. 38 (1990) 2435–2453. doi:10.1016/0956-7151(90)90255-F.